Principle and Design of a Single-phase Inverter-Based Grounding System for Neutral-to-ground Voltage Compensation in Distribution Networks

Wang, Wen; Yan, Lingjie; Zeng, Xiangjun; Fan, Bishuang; Guerrero, Josep M.

Published in:
I E E E Transactions on Industrial Electronics

DOI (link to publication from Publisher):
10.1109/TIE.2016.2612180

Publication date:
2017

Document Version
Early version, also known as pre-print

Principle and Design of a Single-phase Inverter Based Grounding System for Neutral-to-ground Voltage Compensation in Distribution Networks

Wen Wang, *Member, IEEE*, Lingjie Yan, Xiangjun Zeng, *Member, IEEE*
Bishuang Fan and Josep M. Guerrero, *Fellow, IEEE*

***Abstract*—Neutral-to-ground overvoltage may occur in non-effectively grounded power systems because of the distributed parameters asymmetry and resonance between Petersen coil and distributed capacitances. Thus, the constraint of neutral-to-ground voltage is critical for the safety of distribution networks. In this paper, an active grounding system based on single-phase inverter and its control parameter design method is proposed to achieve this objective. Relationship between its output current and neutral-to-ground voltage is derived to explain the principle of neutral-to-ground voltage compensation. Then, a practical current detection method is proposed to specify the reference of compensated current. A current control method consisting of proportional resonant (PR) and proportional integral (PI) with capacitive current feedback is then proposed to guarantee sufficient output current accuracy and stability margin subjecting to large range of load change. The PI method is taken as the comparative method and the performances of both control methods are presented in detail. Experimental results prove the effectiveness and novelty of the proposed grounding system and control method.**

***Index Terms*—Current control, distribution networks, flexible grounding method, neutral voltage compensation.**

I. Introduction

EITHER in theory or practice, the major objective of grounding system in distribution networks is to constrain the ground current to extinguish the arcs caused by the single-line-to-ground (SLG) fault. However, the other purpose of grounding system is commonly disregarded, i.e., to control the neutral-to-ground voltage within certain limit [1]. This is critical for the safety of the power system especially when the inherent asymmetry is high.

Inherent asymmetry directly determines the neutral-to-ground voltage in ungrounded system or high resistance grounded (HRG) system [2]. It is caused by the asymmetry of the distributed parameters, i.e., phase-to-ground capacitances and leakage resistances. Several reasons may cause the asymmetry, including inappropriate transposition in overhead lines, single- or two- phase open-circuit, medium voltage (MV) single phase load [3], etc. Moreover, the neutral-to-ground voltage closely relates to the grounding method. Obviously, it is limited to a small value in an effectively grounded system. Whereas, in resonant grounded (RG) system, it may even exceed the line-to-neutral voltage as resonance happens between Peterson coil and distributed capacitances [4]. For the purpose of maintaining power supply reliability and extinguishing fault arcs, most MV distribution networks adopt HRG or RG method, which makes the problem of high neutral-to-ground voltage unavoidable.

Several measures are taken to limit the neutral-to-ground voltage in non-effectively grounded systems [3]. Transposition enhancement is a common method for overhead lines to decrease the asymmetrical voltage. However, this method needs huge amount of work and is complicated to implement. Three phase coupling capacitances are used to balance the distributed capacitances. Nevertheless, it is not flexible enough to adapt the change of operation modes in power system. Improvement of detuning and damping ratio in RG systems can decrease the neutral-to-ground voltage caused by the aforementioned resonance [4]. However, this method is not able to eliminate the neutral-to-ground voltage caused by the asymmetry of distributed parameters.

For the purpose of eliminating the neutral-to-ground overvoltage, an active grounding system is needed with the

Manuscript received March 24, 2016; revised June 6, 2016 and July 25, 2016; accepted August 19, 2016. Date of publication Month xx, 201x; date of current version August 19, 2016. This work was supported in part by the National Natural Science Foundation of China under Award 51407014 and 51425701, in part by the Hunan Provincial Natural Science Foundation of China under Award 2015JJ3009, and in part by the Project Funded by the Hunan Provincial Department of Education under Award 15B007.

W. Wang, L. Yan, X. Zeng, and B. Fan are with the Hunan Provincial Key Laboratory of Smart Grids Operation and Control, School of Electrical and Information Engineering, Changsha University of Science and Technology, Changsha 410000, China (e-mail: ww_csust@126.com; 917005764@qq.com; eexjzeng@hotmail.com; fanbishuang@126.com).

J. M. Guerrero is with the Department of Energy Technology, Aalborg University, 9220 Aalborg, Denmark (e-mail: joz@et.aau.dk).

Color versions of one or more of the figures in this paper are available online at http://ieeexplore.ieee.org.

characteristics of injecting certain currents to the neutral point and make it seem like short-circuited to the ground. Obviously, this system cannot be realized by passive components like resistor, reactor or capacitor. Thus, a single-phase inverter based grounding system is adopted in this paper.

The current detection and control methods are essential to the control system of an inverter. These two aspects are great challenges for the design and implementation of the active grounding system. Regarding to current detection methods, literatures [5]-[10] have introduced several charging current detection methods. In [5], the distributed capacitances are detected by twice changing the Petersen coil inductance and measuring the corresponding neutral-to-ground voltage and Petersen coil current. The charging current can be easily calculated then with the measured parameters and the line-to-neutral voltage. However, this method relies on the existence of Petersen coil, thus cannot be adopted in the active grounding system. Literature [7] has introduced a charging current detection method by the phase voltage of the faulty feeder and the variation of three-phase currents. This method can be easily implemented by feeder terminal units. However, the method employs too many sensors, thus the accuracy is hard to be guaranteed. Bolted connection of one phase to the ground with a fixed resistor and a contactor is introduced in [10] to detect the charging current. This method can easily guarantee the current accuracy. However, it still needs a grounding resistor and the detection procedure is too complicated for the control of active grounding system. Additionally, these methods cannot be used directly to compensate the neutral-to-ground voltage as the current for voltage compensation is not identical to the charging current.

The distribution transformer is always in delta/wye connection, thus the three-phase load of the feeder line has no influence on the zero sequence impedance. As the neutral-to-ground voltage only depends on the zero sequence circuit, the real load of the grounding system is thus the distributed impedance. Obviously, the load is mainly capacitive and is likely to be resonant with the LC filter of the grounding system at around fundamental frequency. This may bring about steady state error and undermine stability margin of the control system. These features complicate the topology and parameter design of the active grounding system controller. Several literatures have addressed the load effect and resonance phenomena, and many effective measures have been proposed [11]-[14]. Literature [11] has proposed a mixed controller of proportional integral differential (PID) and Resonant plus load current feedback, to reduce the steady state error and improve the dynamic response while dealing with different load types. However, the design of the controller parameters are not discussed in detail. Literature [12] has discussed the inherent instability of LCL filter in active power filter and introduced the active damping method of capacitive current feedback (CCF) to improve the stability margin. Degradation method can simplify the design of control system for LCL filter [14]. However, as the load types of the grounding system are different from that of the LCL filter, these methods cannot be adopted without modification.

In this paper, a new grounding system based on single-phase inverter is proposed to flexibly control the neutral-to-ground voltage. The relationship between injected current of the grounding system and the neutral-to-ground voltage is firstly derived. Then, a practical current detection method for compensating the neutral-to-ground voltage is introduced by analyzing that relationship. Furthermore, the load effect and resonance phenomena are addressed in detail, followed by a current control strategy. The controller design method is then presented to fulfill the requirements of the control system. Experimental results for validation of the proposed control topology and design method are subsequently provided.

II. Principle of Active Grounding System

A. Principle of Neutral-to-ground voltage compensation

A typical 10kV non-effectively grounded distribution network [15] with one feeder is studied in this paper. Fig. 1 shows the topology of the distribution network with the proposed active grounding system. Since the 10kV busbar is supplied from the 110kV system via a wye/delta transformer T_d, there is no actual neutral point. Thus, a zigzag/wye transformer T_z is applied to virtualize one, and the grounding system is connected between the point and the ground. Fig. 2 shows the simplified distribution network, where E_A, E_B, E_C are three phase voltages. The distributed capacitance and resistance of phase X (X=A, B or C) are C_X and R_X, respectively. The grounding system is composed of a single-phase full-bridge inverter, a LC-type output filter and a coupling transformer T_i. The DC bus of the inverter is supplied by a three phase uncontrolled rectifier which connects to the secondary windings of T_z. The output current of the system is controlled by the PWM pulses of IGBT to execute compensated current reference detection and neutral-to-ground voltage compensation. The transformer is used to regulate the inverter output voltage and isolate the inverter from the distribution network.

Assume that the inverter output current is totally under control, then the grounding system can be treated as an ideal

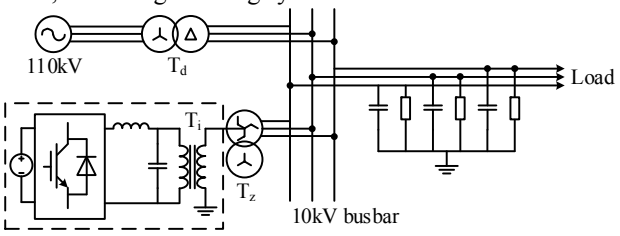

Fig. 1. Topology of distribution network and active grounding system (in dashed box).

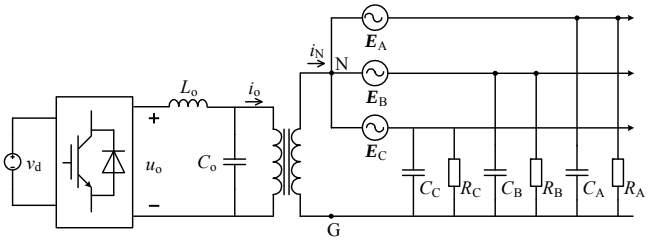

Fig. 2. Simplified distribution network.

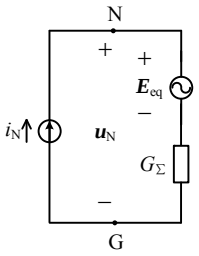

Fig. 3. Simplified circuit of the distribution network.

current source. According to electric circuit theories, the partition of distribution network can be simplified to a voltage source in series with an impedance. Therefore, the circuit of the whole system can be simplified to Fig. 3, where $\boldsymbol{E}_{eq}$ and G_Σ denote the equivalent voltage source and impedance of the distribution network, respectively. They are shown in (1) and (2), where Y_X is the phase-to-ground admittance, i.e., $Y_X=j\omega_0 C_X + 1/R_X$, and ω_0 denotes the fundamental angular frequency.

$$\boldsymbol{E}_{eq} = -G_\Sigma(\boldsymbol{E}_A Y_A + \boldsymbol{E}_B Y_B + \boldsymbol{E}_C Y_C) \tag{1}$$

$$G_\Sigma = \frac{1}{Y_\Sigma} = \frac{1}{Y_A + Y_B + Y_C} \tag{2}$$

Therefore, the relationship between the output current of the grounding system $\boldsymbol{i}_N$ and the neutral-to-ground voltage $\boldsymbol{u}_N$ is

$$\boldsymbol{u}_N = \boldsymbol{i}_N G_\Sigma + \boldsymbol{E}_{eq} = G_\Sigma(\boldsymbol{i}_N - \boldsymbol{E}_A Y_A - \boldsymbol{E}_B Y_B - \boldsymbol{E}_C Y_C). \tag{3}$$

Obviously, if $\boldsymbol{i}_N$ can be controlled to the value in (4), the neutral-to-ground voltage will be zero, which means the asymmetry of distribution network is fully compensated.

$$\boldsymbol{i}_0 = \boldsymbol{E}_A Y_A + \boldsymbol{E}_B Y_B + \boldsymbol{E}_C Y_C \tag{4}$$

It can be further concluded that the compensated current reference also meets (4) while an inductor or resistor is parallel connected to the grounding system. This indicates the grounding system is suitable for distribution network with both HRG and RG grounding. However, as the distributed parameters of the distribution network are complicated to be precisely detected, direct calculation of $\boldsymbol{i}_0$ is not practical.

As the line-to-neutral voltages are balanced and positive-sequenced, $\boldsymbol{E}_B$ and $\boldsymbol{E}_C$ can be substituted by expressions of $\boldsymbol{E}_A$. Take the initial phase angle of $\boldsymbol{E}_A$ as the zero phase base, i.e., $\boldsymbol{E}_A=E_A\angle 0^\circ$, then (3) can be rewritten to

$$\boldsymbol{u}_N = G_\Sigma(i_N e^{j\theta} - i_0 e^{j\theta_0}). \tag{5}$$

In (5), θ and θ_0 denote the phase angle of $\boldsymbol{i}_N$ and $\boldsymbol{i}_0$, respectively. Therefore, the magnitude of neutral-to-ground voltage can be obtained.

$$u_N(i_N,\theta) = |G_\Sigma|\sqrt{i_N^2 + i_0^2 - 2i_N i_0\cos(\theta-\theta_0)} \tag{6}$$

Take the first-order partial derivative operation of u_N, then the change rate of u_N with the magnitude and phase angle of $\boldsymbol{i}_N$ can be observed.

$$\frac{\partial u_N(i_N,\theta)}{\partial i_N} = |G_\Sigma|\frac{i_N - i_0\cos(\theta-\theta_0)}{\sqrt{i_N^2 + i_0^2 - 2i_N i_0\cos(\theta-\theta_0)}} \tag{7}$$

$$\frac{\partial u_N(i_N,\theta)}{\partial \theta} = |G_\Sigma|\frac{i_N i_0\sin(\theta-\theta_0)}{\sqrt{i_N^2 + i_0^2 - 2i_N i_0\cos(\theta-\theta_0)}} \tag{8}$$

It can be seen from (4) that i_0 and θ_0 are fixed in a specific distribution network. From (7), when we set θ to certain value θ^*, u_N has an inflection point in

$$i_N = i_0\cos(\theta^* - \theta_0). \tag{9}$$

The trend of u_N needs to be discussed under several conditions. If $-\pi/2 \le \theta^*-\theta_0 < \pi/2$, u_N will first decrease then increase when i_N increases from 0 to infinite. The break point is determined by (9). This means u_N has a minimal value at the point. If $\pi/2 \le \theta^*-\theta_0 < 3\pi/2$, u_N will be monotonically increasing. Therefore, u_N has a minimal value at the point determined by (9) as well. From (8), when we set i_N to certain value of i^*, u_N has another inflection point in

$$\theta = \theta_0. \tag{10}$$

B. Compensation Current Detection Method

Comparing (9) with (10), interesting conclusions can be found. Firstly, the inflection point determined by (9) is related to θ^*, which means it changes with the set value of θ. However, the inflection point determined by (10) is independent to i_N. That is to say, whatever value i_N is chosen, the inflection point will not vary. Secondly, θ must be chosen to θ_0 to make the inflection point in (9) equal to the magnitude of $\boldsymbol{i}_0$, which is the compensated current reference; whereas, the inflection point in (10) is right the phase angle of $\boldsymbol{i}_0$. These features can be used to quickly locate the magnitude and phase of $\boldsymbol{i}_0$.

From the analysis above, it can be seen that if sinusoidal currents with any fixed magnitude and changing phases are injected to the neutral, the phase of $\boldsymbol{i}_0$ can be located just by detecting the minimal u_N. Comparatively, only when the phase of the injected current is set to θ_0 could the magnitude of $\boldsymbol{i}_0$ be located in the same way, which is almost impossible as $\boldsymbol{i}_0$ is unknown. This can be seen more directly from the vector diagrams in Fig. 4 and Fig. 5. In these figures, the magnitude of $\boldsymbol{u}_N$ is divided by the magnitude of G_Σ to simplify the analysis.

Fig. 4 shows the variation of $\boldsymbol{u}_N$ when different magnitudes of $\boldsymbol{i}_N$ are chosen. Two typical values are chosen, that is, i_{N1} and i_{N2}. The first one is smaller than i_0, and the second is larger. Assuming the two groups of $\boldsymbol{i}_N$ with fixed magnitudes are

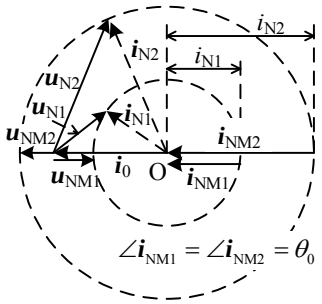

Fig. 4. Vector diagram of $\boldsymbol{u}_N$ when i_N varies.

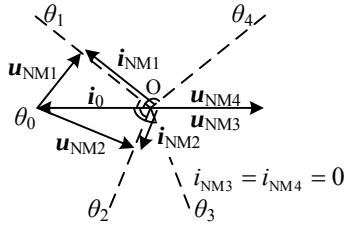

Fig. 5. Vector diagram of $\boldsymbol{u}_N$ when θ varies.

injected to the neutral, the corresponding groups of vector $\boldsymbol{u}_N$ can be drawn according to (5). Obviously, the initial points of them are fixed to the tail of $\boldsymbol{i}_0$, and the terminal points of them follow the circles in dash line, as $\boldsymbol{u}_{N1}$ and $\boldsymbol{u}_{N2}$ illustrate. By the laws of geometry, the vector in radial direction has the minimal magnitude in both groups, shown by $\boldsymbol{u}_{NM1}$ and $\boldsymbol{u}_{NM2}$. The corresponding injected current vectors are shown by $\boldsymbol{i}_{NM1}$ and $\boldsymbol{i}_{NM2}$. Obviously, they have the same phase angle with θ_0, thus the conclusion can be drawn that no matter how much the injected current magnitude is chosen, the phase angle of the current corresponding to the minimal magnitude of $\boldsymbol{u}_N$ is just the same with θ_0.

Fig. 5 shows the variation of $\boldsymbol{u}_N$ when different phase angles of $\boldsymbol{i}_N$ are chosen. θ_1 to θ_4 are chosen for comparison; two of them have less than $\pi/2$ angle difference to $\boldsymbol{i}_0$ (θ_1 and θ_2), and the others larger (θ_3 and θ_4). Assuming that four groups of $\boldsymbol{i}_N$ with these phase angles are injected to the neutral, the corresponding groups of $\boldsymbol{u}_N$ can be drawn according to (5). For the first two groups of $\boldsymbol{u}_N$, it is obvious that the minimal magnitude occurs when $\boldsymbol{u}_N$ is vertical to $\boldsymbol{i}_N$, as shown by $\boldsymbol{u}_{NM1}$ and $\boldsymbol{u}_{NM2}$. The injected current vectors corresponding to them are $\boldsymbol{i}_{NM1}$ and $\boldsymbol{i}_{NM2}$, respectively. For the other two angles of $\boldsymbol{i}_N$, the minimal u_N occurs only when i_N comes to zero, as $\boldsymbol{u}_{NM3}$ and $\boldsymbol{u}_{NM4}$ show. It can be seen that none of the current magnitudes corresponding to the minimal u_N is identical to θ_0.

It can be concluded that when the magnitude of $\boldsymbol{i}_N$ is preset and fixed to certain value large enough for precise detection, the angle of $\boldsymbol{i}_0$ can be located via detecting minimal u_N; whereas, if the angle of $\boldsymbol{i}_N$ is preset and fixed to certain value, the magnitude of $\boldsymbol{i}_0$ can hardly be located by detecting minimal u_N. Therefore, a convenient way to detect the magnitude and phase of $\boldsymbol{i}_0$ can be drawn.

Firstly, preset the magnitude of $\boldsymbol{i}_N$ to certain value; search the minimal magnitude of $\boldsymbol{u}_N$ by changing the angles of $\boldsymbol{i}_N$ and injecting them to the neutral; the phase angle corresponding to minimal u_N is namely θ_r. Then, fix the angle of $\boldsymbol{i}_N$ to θ_r; search the minimal magnitude of $\boldsymbol{u}_N$ again by changing the magnitudes of $\boldsymbol{i}_N$ and injecting them to the neutral; the corresponding magnitude is namely i_r. Finally, the current reference for compensating the distribution network asymmetry is with the magnitude of i_r and the angle of θ_r.

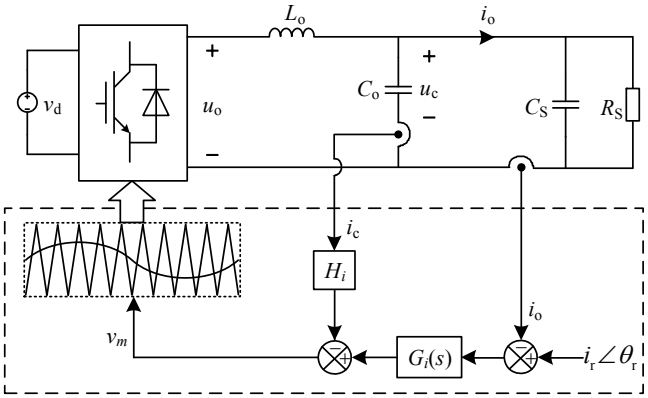

Fig. 6. Simplified main circuit.

III. Current Control Strategy

A. Control model

As the line-to-neutral voltages rarely change, we consider them to be zero during the control analysis. Thus, the voltage source $\boldsymbol{E}_{eq}$ in Fig. 3 can be treated as short-circuited. By converting the equivalent impedance G_Σ to the converter side of the coupling transformer as C_S and R_S, the main circuit is thus simplified to Fig. 6.

While conducting the current control, a typical method is to use output current feedback. Fig. 7 shows the feedback control diagram of the system, where Δi_o is the output current error. From this diagram, the relationship between modulation signal v_m and inverter output current i_o is presented by G_1.

$$G_1(s)=\frac{i_o(s)}{v_m(s)}=\frac{K_{pwm}(sR_sC_s+1)}{s^2R_sL_o(C_o+C_s)+sL_o+R_s} \tag{11}$$

As L_o, the inductance of LC filter, is usually set to be small, resonance occurs when the frequency comes to ω_r.

$$\omega_r=\sqrt{\frac{1}{L_o(C_o+C_s)}} \tag{12}$$

Fig. 8 shows Bode diagram of G_1 with typical parameters listed in TABLE I. The parameters of distribution network are the same as a real one with 50A charging current. In Fig. 8, resonance in ω_r can be obviously observed. This resonance brings about -180° phase shift to G_1. The resonant frequency is related to C_s, which varies with the distribution network parameters. If the frequency locates in the low frequency band,

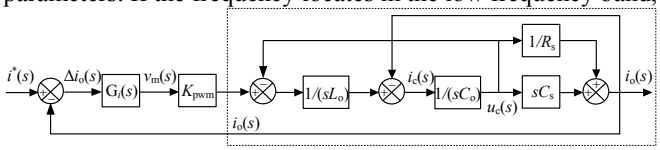

Fig. 7. Control diagram with only output current feedback.

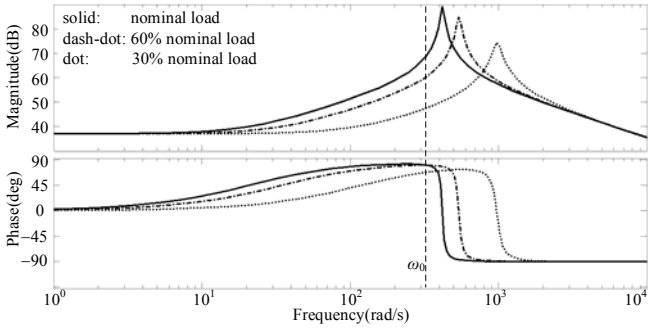

Fig. 8. Bode diagrams of $G_1(s)$ when C_s varies.

TABLE I
System Parameters

	Parameters	Values
Distribution Network	Damping ratio d	0.08
	Phase-to-ground capacitance C_A, C_B	8.76 uF
	Phase-to-ground capacitance C_C	14 uF
	Fundamental frequency f_0	50 Hz
	Phase-to-neutral voltage E_X	10.5/√3 kV
Grounding system	Transformer ratio	10.5/√3:0.32
	Output inductance L_o	0.5 mH
	Output capacitance C_o	50 uF
	Inverter gain K_{pwm}	300
	DC voltage	600 V

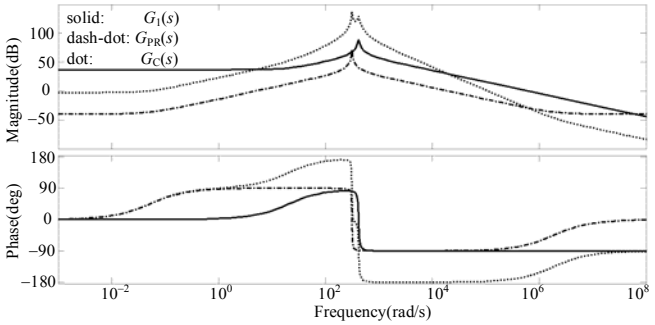

Fig. 9. Bode diagrams of $G_1(s)$, $G_{PR}(s)$ and $G_C(s)$.

the steady state error might increase. Fig. 8 also shows Bode diagrams as C_s varies in nominal, 60%, and 30% of nominal. Magnitude in fundamental angular frequency decreases from 67.7 dB to 47.1 dB as C_s decreases, which means significant increase of steady state error at fundamental frequency. Moreover, if the resonant frequency locates in the medium band, the phase margin of the control system might decrease. In order to guarantee minimal steady state error in fundamental frequency, the proportional resonance controller is usually adopted [16]. However, the controller also brings about -180° phase shift, as the Bode diagrams in Fig. 9 show. Since the crossover frequency ω_c is always in the medium band, which is probably larger than ω_r and ω_0, the phase margin of the whole control system $G_C(s) = G_{PR}(s)G_1(s)$ approaches zero, which makes the system easily unstable.

B. Capacitive current feedback

From the analysis above, the resonance should be carefully damped to meet control performance requirements [17]-[19]. This paper presents an active damping method that flexibly damps the resonance without any loss as illustrated in Fig. 10. In this method, the current of C_o is feedback to the control loop with a ratio of H_i. Therefore, the transfer function from current regulator output v_r to output current i_o is

$$G_2(s) = \frac{i_o(s)}{v_r(s)} = \frac{K_{pwm}(sR_sC_s+1)}{s^2R_sL_o(C_o+C_s)+s(L_o+K_{pwm}H_iR_sC_o)+R_s}. \quad (13)$$

Obviously, the capacitive current feedback (CCF) introduces a ratio of $K_{pwm}H_iR_sC_o$ to the s term of the denominator. As a result, the magnitude of G_2 decrease significantly at the original resonant frequency ω_r, which effectively damps the control system. Fig. 11 shows both Bode diagrams of the original system and damped system. It is clear that CCF damps the magnitude at the resonant frequency and enhances the phase margin of the system. The damping degree rises as the feedback ratio H_i increases, which means smaller magnitude in resonant frequency and larger phase margin. Meanwhile, the CCF also brings smaller magnitude at fundamental frequency, which

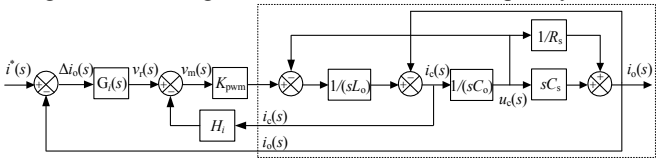

Fig. 10. Control diagram with proposed CCF.

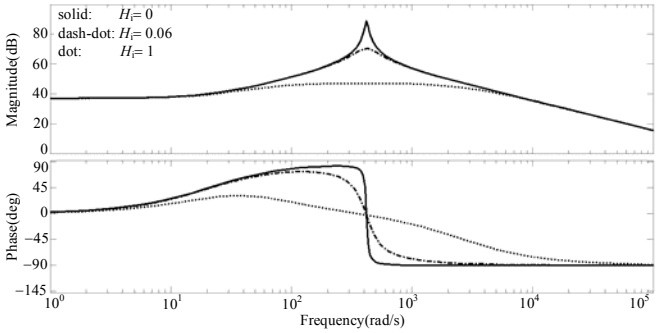

Fig. 11. Bode diagrams comparison of $G_1(s)$ and $G_2(s)$ with various H_i.

undermines the steady state performance. Therefore, the current regulator must have significant magnitude at fundamental frequency to achieve minimal steady state error.

C. Current Regulator

PR controller with damped form is used in current regulator to enhance the steady state performance and adapt to the power system frequency variation.

$$G_{PR}(s) = k_{p\_PR} + \frac{2k_r\omega_i s}{s^2+2\omega_i s+\omega_0^2} \quad (14)$$

The magnitude of PR controller in both low and high frequency band is determined only by the proportional ratio k_{p_PR}. To avoid the high order harmonic interference, the crossover frequency of the whole control system is always set in the medium band, typically 1/10 of the switching frequency [20]. In order to fulfill this requirement, k_{p_PR} should not be too large. However, the limited k_{p_PR} may not ensure the system stability as shown later. Therefore, PR controller can hardly meet both the requirements of anti-interference and control system stability. Thus, an additional PI controller is introduced.

$$G_{PI}(s) = k_{p\_PI} + \frac{k_i}{s} \quad (15)$$

The compound controller has the advantage of infinite gain at zero frequency and fixed gain in high frequency. Thus, it is easy to enlarge the system gain in low band and avoid its influence to the crossover frequency. The integral ratio k_i should also be carefully chosen to prevent the -90° phase shift in low frequency from undermining phase margin. Consequently, the current regulator and the open-loop transfer function of the whole system can be described as follows.

$$G_i(s) = G_{PR}(s)G_{PI}(s) \quad (16)$$

$$G_t(s) = G_{PR}(s)G_{PI}(s)G_2(s) \quad (17)$$

IV. Control Parameter Design

A. PWM constraint

The PWM constraint is firstly described so that the conclusion can be used in the following analysis. For a realizable pulse width modulation, the modulation waveform should only cross the carrier waveform once in a switching period. That is to say, the maximum frequency of modulation waveform should not exceed the switching frequency [21]. Therefore, the following expression stands.

$$H_i \le \frac{4 f_{sw} L_o}{K_{pwm}} \tag{18}$$

B. PI controller

As the PI controller has −90° phase shift in low frequency band, which might decrease the phase margin of the control system, the corner frequency of the controller should be much smaller than the crossover frequency. That is

$$\frac{k_i}{k_{p\_PI}} \ll \omega_c . \tag{19}$$

The proportional ratio k_{p_PI} can be adjusted to slightly modify the performance of the whole system. In order to simplify parameter design, k_{p_PI} is set to one, so that in the medium frequency band and above, the effect of PI controller is negligible. Therefore, the following expression of integral ratio stands.

$$k_i \ll \omega_c \tag{20}$$

C. Crossover frequency

To prevent phase shift of PR controller from decreasing the phase margin, the crossover frequency ω_c is always set to be in the medium band far away from the fundamental frequency. Thus, the PR controller can be simplified to a pure amplifier loop at crossover frequency determined by the proportional ratio. As analyzed above, the PI controller at the crossover frequency can be treated as a proportional loop with the gain of k_{p_PI}. Thus, the gain of current controller at the crossover frequency is

$$\left|G_i(j\omega_c)\right| = \left|G_{PR}(j\omega_c)G_{PI}(j\omega_c)\right| = k_{p\_PR} . \tag{21}$$

As the magnitude of open-loop gain at the crossover frequency is unity, the relationship of ω_c, k_{p_PR} and H_i can be obtained by the following equation.

$$\left|G_t(j\omega_c)\right| = 1 \tag{22}$$

Using (13) to (21), following equation can be drawn.

$$\left|\frac{k_{p\_PR}K_{pwm}(1+j\omega_c R_s C_s)}{R_s[1-\omega_c^2 L_o(C_o+C_s)]+j\omega_c(L_o+K_{pwm}H_i R_s C_o)}\right| = 1 \tag{23}$$

Notice that the distribution network damping ratio $d = 1/(\omega_o R_s C_s)$ has typical values of 0.03 to 0.08. It is reasonably negligible comparing to one. The capacitance of LC filter C_o is always set to be much smaller than the distributed capacitance C_s. Thus, (23) can be rewritten to

$$\left|\frac{k_{p\_PR}(1-jd\frac{\omega_0}{\omega_c})}{\frac{d\omega_0 L_o}{K_{pwm}}+H_i\frac{C_o}{C_s}-j\frac{1}{K_{pwm}}(\frac{1}{\omega_c C_s}-\omega_c L_o)}\right| = 1 . \tag{24}$$

Considering the reactance of C_s at the crossover frequency is far less than that of L_o, thus, (24) can be further simplified to

$$k_{p\_PR}^2 - H_i^2(\frac{C_o}{C_s})^2 = (\frac{\omega_c L_o}{K_{pwm}})^2 . \tag{25}$$

It can be observed from (18) that H_i is limited to a small value. Furthermore, C_o is much smaller than C_s, thus the following expression stands.

$$k_{p\_PR} = \frac{\omega_c L_o}{K_{pwm}} \tag{26}$$

As the zero-frequency gain of $G_2(s)$ is K_{pwm}/R_s from (13), if single PR controller with certain proportional ratio of (26) is used, the whole system gain at zero-frequency will be

$$\frac{\omega_c L_o}{K_{pwm}}\frac{K_{pwm}}{R_s} = \frac{\omega_c L_o}{R_s} . \tag{27}$$

With the typical values listed in TABLE I, it can be seen that $\omega_c L_o / R_s$ is less than one. Thus, the gain of the control system with single PR controller in zero frequency is below 0 dB line, which means the whole control system is marginally unstable as shown in Fig. 12. It also shows the stabilized control system after adding PI controller.

D. Steady state error and stability margin constraint

The magnitude of output current error at fundamental frequency is used to describe the steady state error.

$$E_i = \left|\frac{i^*(j\omega_0)-i_o(j\omega_0)}{i^*(j\omega_0)}\right| \tag{28}$$

Assuming that unity feedback of output current is applied, the equation above can be described by open-loop transfer function

$$E_i = \left|1-\frac{G_t(j\omega_0)}{1+G_t(j\omega_0)}\right| = \left|\frac{1}{1+G_t(j\omega_0)}\right| . \tag{29}$$

As the magnitude of PR controller is $k_{p\_PR} + k_r$ at the fundamental frequency, using expressions from (13) to (17), (29) can be transformed to

$$\frac{1}{E_i} = \left|1+\frac{(k_{p\_PR}+k_r)K_{pwm}}{d\omega_0 L_o + K_{pwm}H_i C_o / C_s - j(1/\omega_0 C_s - \omega_0 L_o)}\right| . \tag{30}$$

At fundamental frequency, the reactance of L_o is negligible. Also, $H_i C_o / C_s$ is negligible comparing to $k_{p\_PR} + k_r$. The reactance of C_s at fundamental frequency is also neglected to simplify the analysis. As a result, the steady state error constraint can be described as

$$\frac{k_{p\_PR}+k_r}{H_i} \approx \frac{C_o}{C_s E_i} . \tag{31}$$

Obviously, the gain of current controller at fundamental frequency is inversely proportional to the steady state error. Increasing the gain can obtain better steady state performance. However, the CCF ratio H_i is proportional to the error, which

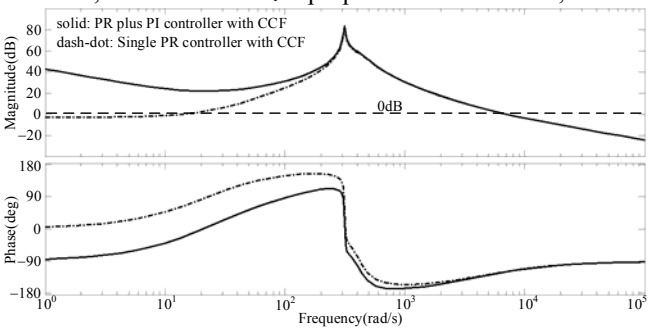

Fig. 12. Bode diagrams of open-loop transfer function with single PR controller and PR plus PI controller.

means better damping of load resonance brings larger steady state error.

It can be seen from Fig. 12 that, with careful selection of controller parameters, the phase of the open-loop transfer function will not exceed the -180° line. These selection tips include that the corner frequency of PI controller should be far away from the crossover frequency, and the resonant cutoff frequency of PR controller should be as small as possible. Consequently, infinite gain margin can be achieved.

While dealing with phase margin constraint, it is necessary to consider the effect of resonant ratio to phase shift. Consider the PR controller at crossover frequency,

$$G_{\mathrm{PR}}(j\omega_{\mathrm{c}}) = k_{\mathrm{p\_PR}} + 2k_{\mathrm{r}}\omega_i / s\,. \tag{32}$$

As is analyzed above, the PI controller can be treated as a pure amplifier loop at the crossover frequency. Therefore, phase margin (*PM*) can be expressed as follows.

$$PM = 180^\circ + \angle G_{\mathrm{PR}}(j\omega_{\mathrm{c}}) + \angle G_2(j\omega_{\mathrm{c}}) \tag{33}$$

Using (13) and (32), considering that the reactance of C_{s} at crossover frequency is negligible, the constraint of phase margin is derived in the Appendix and is expressed as follows.

$$\frac{k_{\mathrm{r}}}{k_{\mathrm{p\_PR}}} \geq \frac{\omega_{\mathrm{c}}(\omega_{\mathrm{c}}L_{\mathrm{o}}C_{\mathrm{s}} + K_{\mathrm{pwm}}C_{\mathrm{o}}H_i \tan PM)}{2\omega_i(\omega_{\mathrm{c}}L_{\mathrm{o}}C_{\mathrm{s}} \tan PM - K_{\mathrm{pwm}}C_{\mathrm{o}}H_i)} \tag{34}$$

V. Parameter Design and Experimental Results

In order to validate the theoretical analysis, comparative investigations are carried out on two control methods of PI and PR plus PI (compound controller) with or without CCF. As stability margin is not easy to be observed in experimental results, Bode diagrams are used to illustrate it. Experiment analysis focuses on the dynamic and steady state performance.

A. Parameter design

According to the theoretical analysis, the parameters of PI and PR controller are constraint by expressions (20), (26), (31) and (34). Thus, the crossover frequency, steady state error and phase margin need to be set forward.

As the switching frequency is fixed to 10 kHz, the crossover frequency is set to 1 kHz. The steady state error is set to 0.5% to guarantee good steady state performance. The phase margin is set to 60° to ensure sufficient stability margin. The corner frequency of PI controller is set to 30 Hz to avoid interference of steady state accuracy and stability margin. Therefore, the parameters of the two controllers can be obtained as in TABLE II. The Bode diagram of the regulated open-loop transfer function is shown in Fig. 13. It can be seen that the crossover frequency of the control system is 7.13×10^3 rad/s, slightly over the set value. The gain at fundamental frequency is 83.3 dB, which means a steady state error of 6.45×10^{-5}, a far smaller value than the set value. This is because the resonant ratio k_{r} is not only determined by the steady state error constraint expression (31), but also *PM* constraint expression (34). The larger k_{r} is chosen here to meet both requirements. The phase of open-loop function does not exceed the -180° line, validating that the gain margin is infinite. Additionally, the phase margin is 61.3°, which is close to the set value.

TABLE II
CONTROL PARAMETERS

	Parameters	Values
PI controller	Proportional ratio $k_{\mathrm{p\_PI}}$	1
	Integral ratio k_{i}	189
PR controller	Proportional ratio $k_{\mathrm{p\_PR}}$	0.01
	Resonant ratio k_{r}	6.4
	Damping ratio ω_{i}	3.14
CCF	Feedback ratio H_{i}	0.06

Comparative Bode diagrams of PI and compound controller are also shown in Fig. 13, both without CCF. Obviously, the former has greater crossover frequency and phase margin, indicating quicker response and better stability than the proposed one. However, it is not able to effectively suppress the harmonics of the output currents. The compound controller without CCF suffers from the -180° phase shift of load resonance thus is not stable because of negative gain margin.

The voltage and current ratings of the proposed grounding system also need to be discussed. From the system topology, the voltage rating relates to the neutral-to-ground voltage illustrated in (1) and (2). The compensated current of the grounding system is determined by the asymmetry of the distributed parameters, which is illustrated in (4). From these expressions, it can be observed that the worst case occurs in two-phase open-circuit condition. In this condition, the neutral voltage rises to line-to-neutral voltage and the compensated current reference reaches 1/3 of the system charging current. Therefore, the nominal voltage is identical to the line-to-neutral voltage and the nominal current is set to 1/3 of the system charging current. Please note that it is not the objective of the proposed grounding system to compensate the ground current in SLG fault. Actually, parallel connected Petersen Coil is needed to provide large reactive power to compensate the ground current which is mainly capacitive.

B. Experimental results

To verify the proposed active grounding system practically, a 100kVA prototype is built in laboratory, based on the topology in Fig. 1 and parameters in TABLE I. Slight change has been made to the topology that a step-up transformer is used to convert a 380V power supply to 10kV, substituting the 110kV supply and transformer T_{d}. The inverter of the grounding system mainly consists of two parallel connected single-phase IPM modules FF450R12ME4 from Infineon. The capacity of coupling transformer T_{i} is 100kVA. The inherent phase-to-ground capacitance and resistance is realized by two groups of capacitors and resistors corresponding to nominal

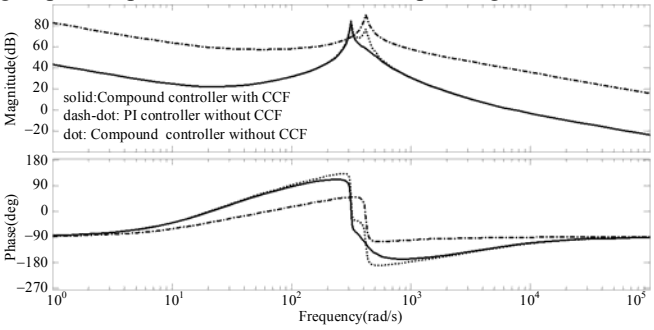

Fig. 13. Bode diagrams of open-loop transfer function with compound controller and CCF.

value in TABLE I and 30% of them to represent two different load levels. The control methods discussed above are executed in a digital signal processor TMS320F28335 development platform with carrier waveform frequency of 10 kHz. In the experimental process, a step-up of load from 0 to 30% nominal load is firstly carried out, followed by another step-up from 30% nominal load to 100%. The controller of PI without CCF is taken as the comparative controller to the proposed compound controller with CCF. The reference values of output current are detected by the compensation current detection method proposed in Section II. Dynamic waveforms subjecting to the two step-ups with different controllers are shown in Fig. 14 to Fig. 17. The error of the output current Δi_o (see Fig. 7) is shown for explicit observation of the control performance.

From the dynamic waveforms of output currents, it can be seen that both methods can reach stable system output. The adjusting time of PI controller is slightly smaller than the proposed method because of larger bandwidth of PI control system as shown in Fig. 13. However, Fig. 14 and Fig. 15 indicate that PI method suffers from larger overshoot than the proposed method with almost twice the value of output current and neutral-to-ground voltage, which is harmful for the safety of power supply apparatus. It can be seen from Fig. 16 that with PI method the percentage error of output current is smaller subjecting to 100% nominal load than 30% of nominal load, which can be explained by the load effect in section III.

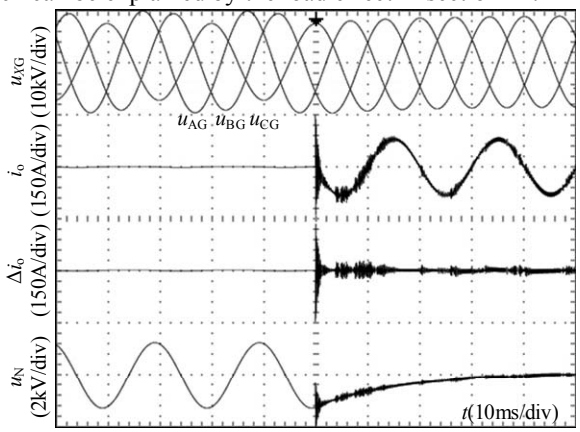

Fig. 14. Dynamic waveforms subjecting to load step-up from 0 to 30% nominal load with PI controller.

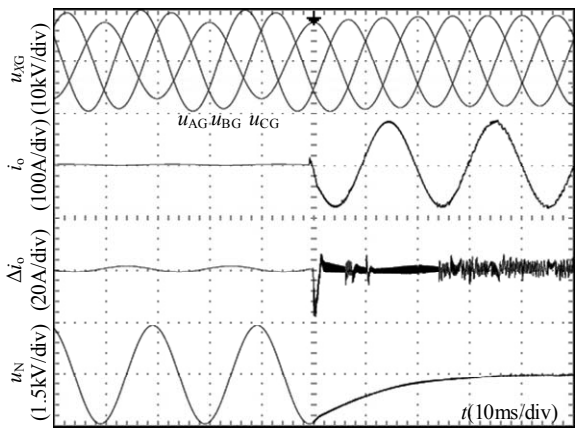

Fig. 15. Dynamic waveforms subjecting to load step-up from 0 to 30% nominal load with proposed method.

Comparatively, as shown in Fig. 17, with the proposed controller, the percentage errors of output current before and after load change are relatively closer than that of PI method, which indicates the proposed controller is more suitable for load change than PI controller. It should be noticed that the dynamic process of neutral-to-ground voltage after load change are longer than that of output current, due to the large time constant of the load.

Fig. 18 and Fig. 19 show steady state waveforms of the two control methods subjecting to 100% nominal load. Greater error in the fundamental components of output current error and neutral-to-ground voltage can be observed with PI controller than the proposed method. Spectrum analysis indicates that the neutral-to-ground voltage subjecting to the proposed method mainly contain harmonics with integrally multiple orders of the switching frequency. The neutral-to-ground voltage waveform in Fig. 18 shows a reduced voltage of around 42V subjecting to PI method. Spectrum analysis indicates the total harmonic distortion (THD) of the output current as 5.1%. From the output current and current error waveform in Fig. 19, it can be seen that the steady state error of the proposed method reaches 3%. The neutral-to-ground voltage is reduced by the grounding system with the proposed method to around 21V, better than PI method. The THD of the output current with the proposed method reaches 3.0%, also better than that of PI method. Both

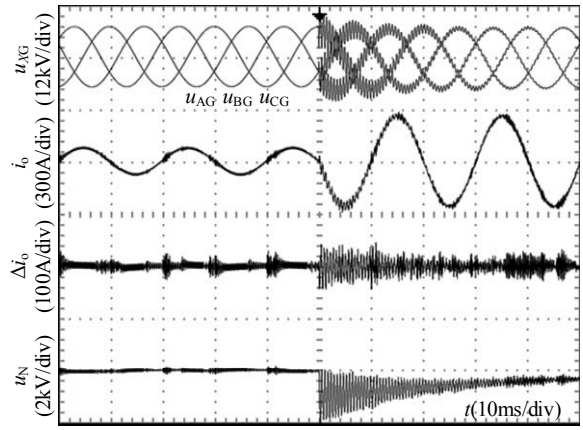

Fig. 16. Dynamic waveforms subjecting to load step-up from 30% nominal load to 100% with PI controller.

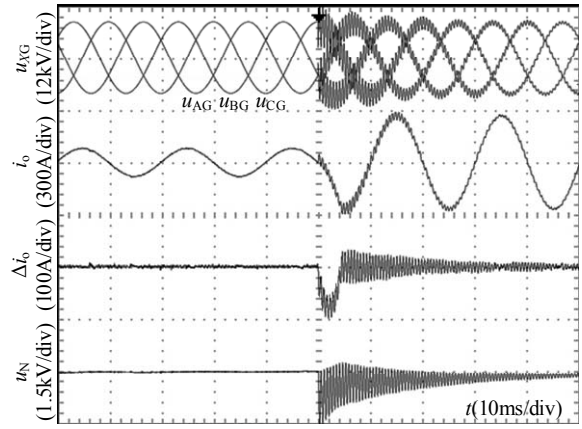

Fig. 17. Dynamic waveforms subjecting to load step-up from 30% nominal load to 100% with proposed method.

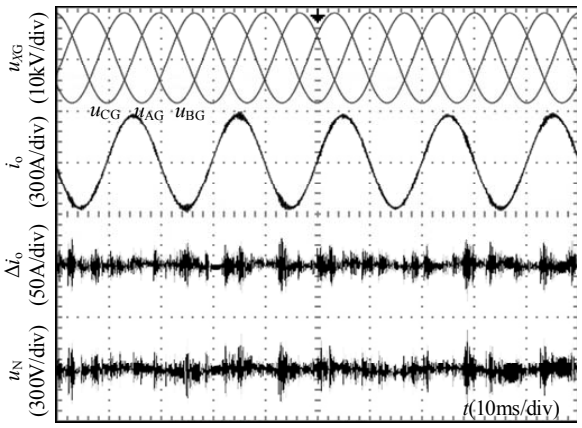

Fig. 18. Steady state waveforms subjecting to 100% nominal load with PI controller.

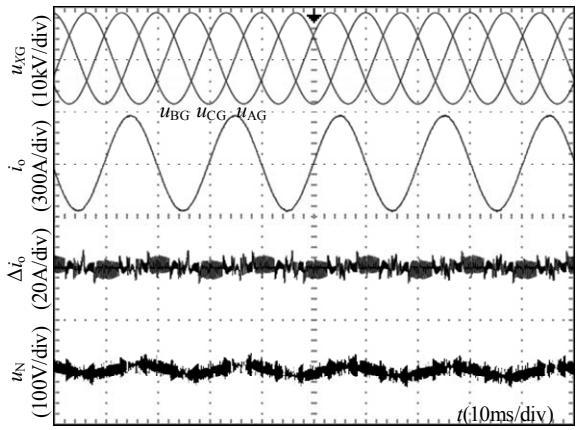

Fig. 19. Steady state waveforms subjecting to 100% nominal load with proposed method.

of the neutral-to-ground voltage and output current THD indicate a better steady state performance of the proposed method than PI method.

VI. Conclusion

The proposed active grounding system is able to effectively constrain the neutral-to-ground voltage to avoid possible overvoltage caused by asymmetrical distributed parameters or resonance between Petersen coil and phase-to-ground capacitance. A practical compensation current detection method is proposed which firstly specifies the phase angle, and then the magnitude of the current reference. Current control method is also presented which consists of a PR plus PI controller and capacitive current feedback. The proposed control method is suitable for large range of load change and is immune to possible resonance between load capacitance and output LC filter inductance. Experimental results show that the proposed control method has better performance in dynamic and steady state than PI method.

Appendix

The limit of k_r/k_{p_PR} constraint by phase margin (PM) is derived here. The expression of $G_2(j\omega_c)$ can be easily obtained from (13). Dividing both the nominator and denominator by $j\omega_c R_s C_s$, and considering that $C_o << C_s$ and substituting d for $1/(\omega_0 R_s C_s)$, it yields

$$G_2(j\omega_c)=\frac{K_{pwm}(1-jd\frac{\omega_0}{\omega_c})}{\frac{L_o+K_{pwm}H_iR_sC_o}{R_sC_s}+j(\omega_cL_o-\frac{1}{\omega_cC_s})}. \quad (A.1)$$

As the reactance of C_s at crossover frequency is much smaller than that of L_o and $d\omega_0/\omega_c << 1$, (A.1) can be rewritten as

$$\angle G_2(j\omega_c)=-\arctan\frac{\omega_cL_oR_sC_s}{L_o+K_{pwm}H_iR_sC_o}. \quad (A.2)$$

Using (A.2) and (32), (33) can be rewritten as

$$PM=180^\circ-\arctan\frac{2k_r\omega_i}{k_{p\_PR}\omega_c}-\arctan\frac{\omega_cL_oR_sC_s}{L_o+K_{pwm}H_iR_sC_o}. \quad (A.3)$$

Equation (A.3) can be rewritten by an inequality as

$$\arctan\frac{2k_r\omega_i}{k_{p\_PR}\omega_c}+\arctan\frac{\omega_cL_oR_sC_s}{K_{pwm}H_iR_sC_o}>180^\circ-PM. \quad (A.4)$$

Applying the tangent function operation to both sides of (A.4), following expression can be obtained.

$$\frac{k_r}{k_{p\_PR}}\geq\frac{\omega_c(\omega_cL_oC_s+K_{pwm}C_oH_i\tan PM)}{2\omega_i(\omega_cL_oC_s\tan PM-K_{pwm}C_oH_i)} \quad (A.5)$$

References

[1] *IEEE Recommended Practice for Grounding of Industrial and Commercial Power Systems*, IEEE Std. 142-2007, 2007.

[2] L. J. Kingrey, R. D. Painter, and A. S. Locker, "Applying High-Resistance Neutral Grounding in Medium-Voltage Systems," *IEEE Trans. Ind. App.*, vol. 47, no. 3, pp. 1220– 1231, May 2011.

[3] X. Zeng, Y. Xu, and Y. Wang, "Some novel techniques for insulation parameters measurement and Petersen-coil control in distribution networks," *IEEE Trans. Ind. Electron.*, vol. 57, no. 4, pp. 1445–1451, Apr. 2010.

[4] A. Kalyuzhny, "Analysis of Temporary Overvoltages During Open-Phase Faults in Distribution Networks With Resonant Grounding," *IEEE Trans. Power Del.*, vol.30, no.1, pp.420-427, Feb. 2015.

[5] X. Lin, J. Huang, and S. Ke, "Faulty Feeder Detection and Fault Self-Extinguishing by Adaptive Petersen Coil Control," *IEEE Trans. Power Del.*, vol.26, no.2, pp.1290-1291, Apr. 2011.

[6] M. Brenna, E. D. Berardinis, L. D. Carpini, P. Paulon, P. Petroni, G. Sapienza, G. Scrosati, and D. Zaninelli, "Petersen Coil Regulators Analysis Using a Real-Time Digital Simulator," *IEEE Trans. Power Del.*, vol.26, no.3, pp.1479-1488, July 2011.

[7] X. Zeng, K. K. Li, W. L. Chan, S. Su, and Y. Wang, "Ground-Fault Feeder Detection With Fault-Current and Fault-Resistance Measurement in Mine Power Systems," *IEEE Trans. Ind. App.*, vol. 44, no. 2, pp. 424– 429, Mar. 2008.

[8] J. Tian, Q. Chen, L. Cheng, and Y. Zhang, "Arc-suppression coil based on transformer with controlled load," *IET Elect. Power App.*, vol.5, no.8, pp.644-653, September 2011.

[9] X. Chen, B. Chen, C. Tian, J. Yuan, and Y. Liu, "Modeling and Harmonic Optimization of a Two-Stage Saturable Magnetically Controlled Reactor for an Arc Suppression Coil," *IEEE Trans. Ind. Electron.*, vol.59, no.7, pp.2824-2831, July 2012

[10] D. Paul, P. E. Sutherland, and S. A. R. Panetta, "A Novel Method of Measuring Inherent Power System Charging Current," *IEEE Trans. Ind. App.*, vol. 47, no. 6, pp. 3230– 3240, Nov. 2011.

[11] D. Dong, T. Thacker, R. Burgos, F. Wang, and D. Boroyevich, "On zero steady-state error voltage control of single-phase PWM inverters with different load types," *IEEE Trans. Power Electron.*, vol. 26, no. 11, pp. 3285– 3297, Nov. 2011.

[12] Y. Tang, P. C. Loh, P. Wang, F. H. Choo, F. Gao, and F. Blaabjerg, "Generalized design of high performance shunt active power filter with output LCL filter," *IEEE Trans. Ind. Electron.*, vol. 59, no. 3, pp. 1443–1452, Mar. 2012.

[13] F. Liu, Y. Zhou, S. Duan, J. Yin, B. Liu, and F. Liu, "Parameter Design of a Two-Current-Loop Controller Used in a Grid-Connected Inverter System With LCL Filter," *IEEE Trans. Ind. Electron.*, vol. 56, no. 11, pp. 4483–4491, Nov. 2009.
[14] G. Shen, X. Zhu, J. Zhang, and D. Xu, "A New Feedback Method for PR Current Control of LCL-Filter-Based Grid-Connected Inverter," *IEEE Trans. Ind. Electron.*, vol. 57, no. 6, pp. 2033–2041, Jun. 2010.
[15] X. Dong and S. Shi, "Identifying Single-Phase-to-Ground Fault Feeder in Neutral Noneffectively Grounded Distribution System Using Wavelet Transform," *IEEE Trans. Power Del.*, vol. 23, no. 4, pp. 1829-1837, Oct. 2008.
[16] A. Kuperman, "Proportional-Resonant Current Controllers Design Based on Desired Transient Performance," *IEEE Trans. Power Electron.*, vol. 30, no. 10, pp. 5341–5345, Oct. 2015.
[17] R. Peña-Alzola, M. Liserre, F. Blaabjerg, R. Sebastián, J. Dannehl, and F. W. Fuchs, "Analysis of the Passive Damping Losses in LCL-Filter-Based Grid Converters," *IEEE Trans. Power Electron.*, vol. 28, no. 6, pp. 2642–2646, Jun. 2013.
[18] W. Wu, Y. He, T. Tang, and F. Blaabjerg, "A New Design Method for the Passive Damped LCL and LLCL Filter-Based Single-Phase Grid-Tied Inverter," *IEEE Trans. Ind. Electron.*, vol. 60, no. 10, pp. 4339–4350, Oct. 2013.
[19] M. Liserre, R. Teodorescu, and F. Blaabjerg, "Stability of photovoltaic and wind turbine grid-connected inverters for a large set of grid impedance values," *IEEE Trans. Power Electron.*, vol. 21, no. 1, pp. 263–272, Jan. 2006.
[20] Erickson and D. Maksimovic, *Fundamentals of Power Electronics*, 2nd ed. Norwell, MA, USA: Kluwer, 2001, pp. 331–408.
[21] C. Bao, X. Ruan, X. Wang, W. Li, D. Pan, and K. Weng, "Step-by-Step Controller Design for LCL-Type Grid-Connected Inverter with Capacitor–Current-Feedback Active-Damping," *IEEE Trans. Power Electron.*, vol. 29, no. 3, pp. 1239 - 1253, Mar. 2014.

Wen Wang (M'14) received the B.S. and Ph.D. degrees in electrical engineering from Hunan University, Changsha, China, in 2008 and 2013, respectively.

Since 2013, he has been an Assistant Professor with the School of Electrical and Information Engineering, Changsha University of Science and Technology, Changsha, China. In 2016, he is a Guest Researcher in the Department of Energy Technology, Aalborg University, Aalborg, Denmark. His current research interests include power electronics, grounding methods in distribution networks.

Lingjie Yan was born in Hubei Province, China, in 1990. He received the B.S. degree in electrical engineering and automation from Huazhong University of Science and Technology, Wuhan, China, in 2010. He is currently working toward his M.S. degree in electrical engineering at Changsha University of Science and Technology, Changsha, China. His research interests include power electronic technology in flexible grounding system.

Xiangjun Zeng (M'03) received the B.S. degree from Hunan University, Changsha, China, in 1993, the M.S. degree from Wuhan University, Wuhan, China, in 1996, and the Ph.D. degree from Huazhong University of Science and Technology, Wuhan, China, in 2001, all in electrical engineering.

He worked as post-doctoral fellow in Xuji Relay Company and the HongKong Polytechnic University and a Visiting Professor at Nanyang Technological University, Singapore, Singapore. He is now a Professor and Dean of the School of Electrical and Information Engineering, Changsha University of Science and Technology, Changsha, China. His research interests include real-time computer application in power systems control and protection.

Bishuang Fan received the B.S. degree in automation control in 2002, and the M.S. degree in automation of electric power system in 2007, both from Changsha University of Science and Technology, Changsha, China, and the Ph.D. degree in control science and engineering from Central South University, Changsha, China, in 2014.

Since 2015, he has been an Associate Professor with the School of Electrical and Information Engineering, Changsha University of Science and Technology, Changsha, China. In 2016, he is a Visiting Scholar at the power electronics laboratory in the Department of Electrical Engineering and Computer Science, University of Tennessee, Tennessee, USA. His current research interests include power conversion technologies.

Josep M. Guerrero (S'01-M'04-SM'08-FM'15) received the B.S. degree in telecommunications engineering, the M.S. degree in electronics engineering, and the Ph.D. degree in power electronics from the Technical University of Catalonia, Barcelona, in 1997, 2000 and 2003, respectively. Since 2011, he has been a Full Professor with the Department of Energy Technology, Aalborg University, Denmark, where he is responsible for the Microgrid Research Program (www.microgrids.et.aau.dk). From 2012 he is a guest Professor at the Chinese Academy of Science and the Nanjing University of Aeronautics and Astronautics; from 2014 he is chair Professor in Shandong University; from 2015 he is a distinguished guest Professor in Hunan University; and from 2016 he is a visiting professor fellow at Aston University, UK, and a guest Professor at the Nanjing University of Posts and Telecommunications.

His research interests is oriented to different microgrid aspects, including power electronics, distributed energy-storage systems, hierarchical and cooperative control, energy management systems, smart metering and the internet of things for AC/DC microgrid clusters and islanded minigrids; recently specially focused on maritime microgrids for electrical ships, vessels, ferries and seaports.

Prof. Guerrero is an Associate Editor for the IEEE TRANSACTIONS ON POWER ELECTRONICS, the IEEE TRANSACTIONS ON INDUSTRIAL ELECTRONICS, and the IEEE Industrial Electronics Magazine, and an Editor for the IEEE TRANSACTIONS on SMART GRID and IEEE TRANSACTIONS on ENERGY CONVERSION. He has been Guest Editor of the IEEE TRANSACTIONS ON POWER ELECTRONICS Special Issues: Power Electronics for Wind Energy Conversion and Power Electronics for Microgrids; the IEEE TRANSACTIONS ON INDUSTRIAL ELECTRONICS Special Sections: Uninterruptible Power Supplies systems, Renewable Energy Systems, Distributed Generation and Microgrids, and Industrial Applications and Implementation Issues of the Kalman Filter; the IEEE TRANSACTIONS on SMART GRID Special Issues: Smart DC Distribution Systems and Power Quality in Smart Grids; the IEEE TRANSACTIONS on ENERGY CONVERSION Special Issue on Energy Conversion in Next-generation Electric Ships. He was the chair of the Renewable Energy Systems Technical Committee of the IEEE Industrial Electronics Society. He received the best paper award of the IEEE Transactions on Energy Conversion for the period 2014-2015, and the best paper prize of IEEE-PES in 2015. In 2014 and 2015 he was awarded by Thomson Reuters as Highly Cited Researcher, and in 2015 he was elevated as IEEE Fellow for his contributions on "distributed power systems and microgrids."